A median redshift of 2.4 for galaxies bright at submillimetre wavelengths

S. C. Chapman*, A. W. Blain*, R. J. Ivison† & Ian R. Smail‡

* *California Institute of Technology, Pasadena, California 91125, USA*
† *Astronomy Technology Centre, Royal Observatory, Blackford Hill, Edinburgh EH9 3HJ, UK*
‡ *Institute for Computational Cosmology, University of Durham, South Road, Durham DH1 3LE, UK*

A significant fraction of the energy emitted in the early Universe came from very luminous galaxies that are largely hidden at optical wavelengths (because of interstellar dust grains); this energy now forms part of the cosmic background radiation at wavelengths near 1 mm (ref. 1). Some submillimetre (submm) galaxies have been resolved from the background radiation[2], but they have been difficult to study because of instrumental limitations[3]. This has impeded the determination of their redshifts (z), which is a crucial element in understanding their nature and evolution[4]. Here we report spectroscopic redshifts for ten submm galaxies that were identified using high-resolution radio observations[5–7]. The median redshift for our sample is 2.4, with a quartile range of 1.9–2.8. This population therefore coexists with the peak activity of quasars, suggesting a close relationship between the growth of massive black holes and luminous dusty galaxies[8]. The space density of submm galaxies at redshifts over 2 is about 1,000 times greater than that of similarly luminous galaxies in the present-day Universe, so they represent an important component of star formation at high redshifts.

The first real insight in the origin of the far-infrared/submm background came with the commissioning of the Submillimeter Common User Bolometric Array (SCUBA) camera on the James Clerk Maxwell Telescope (JCMT). Almost 100% of the submm background has been resolved with the deepest SCUBA maps, which exploit a sensitivity boost from gravitational lenses[2,3,9]. However, the near-infrared/optical faintness of the submm galaxy population conspires with the modest positional precision available from the large (15″) SCUBA beam and the large surface density of unrelated, optically faint galaxies to render positional coincidence alone inadequate to identify counterparts[3,5]. This problem is compounded by the small field of view of SCUBA: compiling large samples of submm galaxies is slow, with roughly one detected every night. Because of these difficulties, robust spectroscopic redshifts have been published for only a handful of submm sources, all atypically bright at optical wavelengths[3,10–12].

Here, we have overcome these problems by taking advantage of 1.4-GHz radio data from the Very Large Array (VLA) radio telescope (Hubble Deep Field[13], SSA13 field[14], ElaisN2 and Lockman fields[7]). These deep images have fine (1–2″) spatial resolution and a large (30′ full-width at half-maximum, FWHM) field of view. The radio data was exploited to follow up SCUBA submm data in the Hubble Deep Field (12-h RA) and SSA13 (13-h RA) fields[5,15,16], and the Lockman (10-h RA) and ElaisN2 (16-h RA) fields[17]. The radio data are sensitive to the synchrotron radio emission from cosmic-ray electrons accelerated in the supernovae explosions of the same high-mass stars that heat the dust and generate the far-infrared/submm emission. Hence using a deep radio image should be an efficient way of pinpointing the positions of many submm galaxies. This is confirmed in fields with both submm and radio observations: radio counterparts brighter than $30\,\mu$Jy can be found for 60–70% of submm galaxies brighter than 5 mJy at 850 μm (which have a surface density[3] of 450 deg^{-2}, and contribute about 20% of the submm background)[7,16]. Moreover, the accurate radio positions mean that SCUBA's efficient 'photometry' mode can be used to search for submm galaxies[5,6,18], raising the detection rate to around ten per night.

Although submm galaxies have faint optical continuum emission[3], the radio-detected samples are sufficiently large to allow efficient, multi-object optical spectroscopy using 10-m telescopes. Slit positions can be assigned accurately, as the radio/submm emission can be located on optical images to within 0.3–0.8″ (ref. 7). Using this approach we targeted 34 radio-detected submm galaxies, mostly brighter than 5 mJy at 850 μm with optical magnitudes in the range $I = 22.2$–26.4, using the Echellette Spectrograph and Imager (ESI) and the Low-Resolution and Imaging Spectrograph (LRIS) on the Keck telescopes (Fig. 1). We measured redshifts for ten submm galaxies, representative of the blank-field population. We have doubled the number of optically bright ($I < 23.5$) submm galaxies with accurate redshifts. Our six redshifts for $I > 23.5$ submm galaxies represent the first redshifts for this class of submm galaxy. The redshifts span the range $z = 0.8$–3.7, with a median of 2.4 and an interquartile range of 1.9–2.8 (Fig. 2). These redshifts allow dust temperatures T_d and bolometric luminosities L_{bol} to be determined (see Table 1), assuming that the tight correlation between far-infrared and radio emission observed at low redshifts[19] remains valid. Typical values are of order 35 K and several $10^{12} L_\odot$ respectively (where $L_\odot$ is the luminosity of the Sun). Note that relativistic electrons accelerated in shocks close to an active galactic nucleus (AGN) should boost the radio flux density above that expected from the standard correlation. If the radio emission is boosted by an AGN then both temperature and luminosity are overestimated. There are no obvious cases in the present sample in this category.

Table 1 Positions and parameters of the observed submillimetre galaxies

Name	Redshift	$S_{850\,\mu m}$ (mJy)	I (mag)	T_d (K)	L_{bol} ($10^{12} L_\odot$)
SMM105224.6+572119	2.429	11.7 ± 3.4*	25.9	21 ± 5	$3.0^{+2.0}_{-0.7}$
SMM163704.3+410530	0.840	11.2 ± 1.6*	21.5	$16^{+4.1}_{-2.2}$	$0.58^{+.32}_{-.34}$
SMM105230.6+572212	2.610	11.0 ± 2.6*	23.0	29 ± 6	$6.9^{+5.9}_{-3.3}$
SMM163650.0+405733	2.376	8.2 ± 1.7*	22.2	54^{+11}_{-7}	45^{+53}_{-19}
SMM123600.2+621047	1.998	7.9 ± 2.4	23.6	37^{+8}_{-4}	10^{+11}_{-4}
SMM131201.2+424208	3.419	6.2 ± 1.2	23.5	48^{+10}_{-7}	20^{+18}_{-7}
SMM105207.7+571907	2.698	6.2 ± 1.6*	26.0	36^{+7}_{-4}	$7.8^{+7.1}_{-2.3}$
SMM131212.7+424423	2.811	5.6 ± 1.9	26.4	54^{+19}_{-10}	30^{+60}_{-16}
SMM163658.8+405733	1.189	5.1 ± 1.4*	22.4	25^{+5}_{-9}	1.5 ± 1.2
SMM105155.7+572312	3.699	4.5 ± 1.3*	24.2	59^{+26}_{-16}	30^{+82}_{-20}

Positions of submm galaxies with redshifts from our survey, along with their measured redshifts, submm fluxes ($S_{850\,\mu m}$) and optical magnitudes (I), inferred dust temperatures (T_d) and bolometric luminosities (L_{bol}). T_d and L_{bol} were calculated from the redshift, submm and radio flux densities, assuming that the far-infrared–radio correlation applies. Sources are in order of decreasing flux density, as in Fig. 1. (SMM163704.3+410530 was previously published in ref. 26.) Submm fluxes for sources in the Lockman (10-h RA) and EliasN2 (16-h RA) fields (indicated by an asterisk) are from ref. 17 and we measured the fluxes for other sources. Six out of ten galaxies have I-band magnitudes fainter than 23.5, consistent with the optical flux distribution of blank-field submm galaxies presented elsewhere[16], and confirming that our sample is representative of the population. The relationship between submm galaxies and other high-redshift populations will be better understood by comparing the strength of the clustering, both within and between the different classes. This will require substantially larger samples than are currently available.
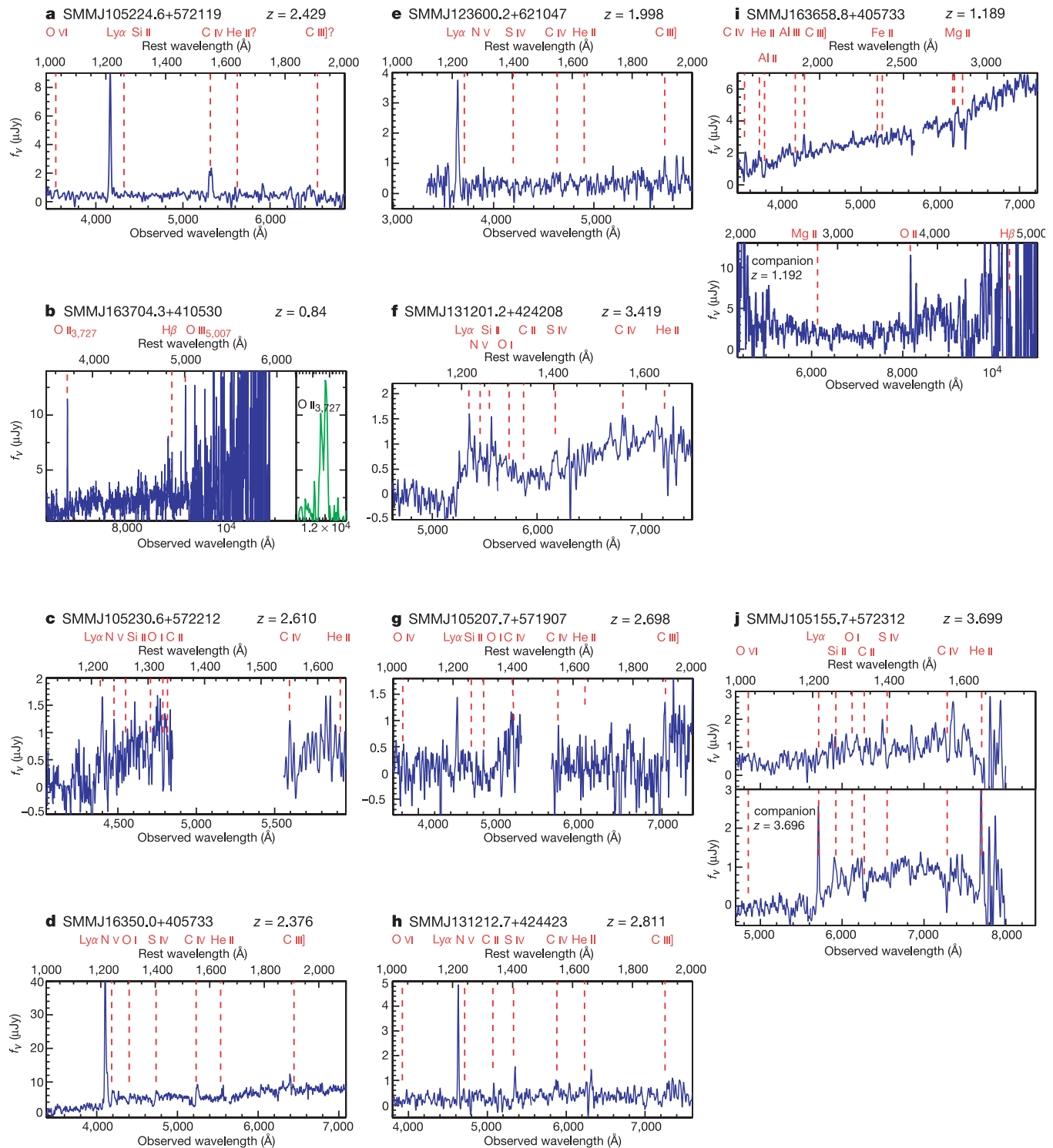
Figure 1 The ten spectra (**a**–**j**) from Table 1 with identified redshifts from the sample of 34 submm galaxies observed, spanning the $I = 22.2$–26.4 range. The redshifts are smoothed to the instrumental resolution. Pilot observations, using Keck's ESI[27] spectrograph on 16 July 2001 in the ELAIS-N2 field[17] yielded three spectra with strong emission lines. Multi-object Keck observations of 31 submm galaxies using LRIS[28] were made on 18–19 March 2002 in light cirrus conditions (with good 0.8″ seeing) in the HDF and SSA13 fields[5,16], and the Lockman Hole and ELAIS-N2 fields[17]. All the spectra probe the observed wavelength range from 0.3–1 μm. Exposure times were 1.5–4.5 h, split into 30-min integrations. Data reduction followed standard techniques using custom Image Reduction Astronomy Facility (IRAF) scripts. One-dimensional spectra were extracted and compared with template spectra and emission-line catalogues to identify redshifts. All identifications are based on multiple lines, most prominently the Lyα line which varies tremendously in both flux (ranging from 1 to 60 μJy) and rest-frame equivalent width (3 to >100 Å). Weaker stellar/interstellar/AGN features and/or continuum breaks were detected in the spectra, strengthening the redshift identifications. Two galaxies at the same redshifts (for sources **i**, **j**) were identified in the vicinity of the ten robust submm sources, as shown for the companions SMMJ105155.7 + 572312-a (one of the few submm galaxies with redshifts showing Lyman-α in absorption) and SMMJ105155.7 + 572312-b. **d**, The highest signal-to-noise spectrum (SMMJ163650 + 405733; ref. 30) includes features indicative of both strong starburst activity (P Cygni wind absorption profiles, stellar/interstellar absorption lines) and a weak AGN, a mix typical of hybrid starburst/Seyfert-2 galaxies. None of our spectra have broad lines like Type-I AGN. Narrow-line Type-II AGN with enhanced N v and/or C iv emission are consistent with half of our spectra (**a**, **d**, **f**, **g**, **h**). Despite this evidence for AGN in these galaxies, AGN appear to be relatively weak in energetic terms as compared to those identified in X-ray or optical surveys. f_ν, specific flux density.

The redshifts impose robust limits to the space densities of submm galaxies in the redshift ranges 0.5–1.2, 1.8–2.8 and 2.8–4 (the gap at $z = 1.2$–1.8 is the 'spectroscopic desert' in which no strong restframe ultraviolet lines are redshifted into the optical window): we calculate $\rho = (3.3 \pm 2.3) \times 10^{-6}\,\mathrm{Mpc}^{-3}$, $(6.5 \pm 2.5) \times 10^{-6}\,\mathrm{Mpc}^{-3}$ and $(2.4 \pm 1.2) \times 10^{-6}\,\mathrm{Mpc}^{-3}$, respectively, assuming a flat (cosmological constant $\Lambda = 0.7$) Universe with current Hubble constant $H_0 = 65\,\mathrm{km\,s}^{-1}\,\mathrm{Mpc}^{-1}$. This compares to a space density of around $10^{-8}\,\mathrm{Mpc}^{-3}$ for low-redshift galaxies with comparable bolometric luminosities greater than $5 \times 10^{12} L_\odot$, comparable to the luminosities of our spectroscopically targeted galaxies at any redshift greater than one. The volume density of very luminous galaxies thus increases almost a thousandfold from $z \approx 0$ to 2.

The relationship between different classes of high-redshift galaxy is critical for our understanding of galaxy evolution. Our spectroscopy shows that the submm galaxies are coeval with the important populations of star-forming galaxies and quasars detected at $z = 2$–3 using optical and X-ray techniques[8,20–22]. We can use their relative space densities to compare and relate these populations. In a $1{,}000\,\mathrm{Mpc}^3$ box at $z \approx 2.5$, there are ten Lyman-break galaxies with $R_{AB} < 25.5$ (about $0.2 \times L^{*}_{1,500}$) and one submm galaxy from our sample (with 850-μm flux >5 mJy), but the single submm galaxy produces a comparable luminosity to the ten Lyman-break galaxies. (Here R_{AB} is the flux normalized magnitude near 6,900 Å; $L^{*}_{1,500}$ is the characteristic luminosity at restframe 1,500 Å, denoting a change in slope in the luminosity function.) Equally, the volume density of submm galaxies is similar to that of narrow-line Type-II AGN selected at these redshifts, from both X-ray and optical surveys, and is an order of magnitude greater than that of bright optical quasars with bolometric magnitude $M_B > -25$ (ref. 8). However, the links between the different classes

of sources all depend critically on whether the activity is intermittent or continuous.

To quantify the whole submm population using this survey we must account for several selection effects. In particular, requiring a radio identification prior to spectroscopy limits the maximum redshift (Fig. 2). Studies of galaxies at low and moderate redshifts suggest that changes in the dust properties, especially the dust temperature T_d, modify the relative strength of the emission in the submm and radio wavebands[23]. The detectability of distant submm galaxies (at a fixed 850-μm flux) in the radio waveband thus depends on the dust temperature: warmer galaxies are detectable at $z \gtrsim 3$, while the radio emission from cooler sources falls below the flux limit at lower redshifts[18]. About 30% of submm galaxies that are brighter than 5 mJy at 850 μm are not detected at radio wavelengths: these galaxies would be lost from our catalogue at $z \approx 2.5$ for the coldest plausible $T_d \approx 25$ K, and at $z > 3$ for the typical $T_d \simeq 35$ K that we find. Hence, we can place only a lower limit on the space density in the highest redshift interval. The density derived at $z = 2$ should be unaffected by the galaxies' detection at radio wavelengths.

We must also consider the completeness of our spectroscopic observations. Although our redshift completeness is relatively high ($\sim 30\%$), we failed to find convincing redshifts for 24 galaxies. However, nine of these have strong single emission line detections which could plausibly be identified as Lyman-α. Some of the remainder without emission lines could lie in the spectroscopic desert, making redshifts difficult to identify. The absence of sources at $z \approx 1.5$ in Table 1 suggests that this effect is probably responsible for some of the incompleteness. Our targets generally have faint ultraviolet continua, and so there is a bias towards identifying redshifts for galaxies with strong emission lines. If the missing galaxies lie outside the spectroscopic desert, but lack strong emission lines, then their radio detection suggests that they probably lie in the same $z = 1$–4 range spanned by the spectroscopically identified sources.

On the basis of bolometric luminosities estimated from our radio and submm measurements and redshifts (Table 1), assuming the far-infrared–radio correlation, we calculate the following luminosity densities from our survey: $\rho_L(0.5 < z < 1.2) = (5 \pm 5) \times 10^6\,L_\odot\,\mathrm{Mpc}^{-3}$, $\rho_L(1.8 < z < 2.8) = (7^{+6}_{-4}) \times 10^7\,L_\odot\,\mathrm{Mpc}^{-3}$ and $\rho_L(2.8 < z < 4.0) = (7^{+10}_{-5}) \times 10^7\,L_\odot\,\mathrm{Mpc}^{-3}$. To translate these values into star-formation densities we must subtract any contribution to the luminosities of these galaxies from the heating of dust by an active galactic nucleus (AGN). The proportion of the submm population detected in deep Chandra and XMM-Newton X-ray surveys, which are sensitive to even dust-obscured AGN[7,20], at flux densities significantly greater than that expected from star formation alone is at most 30%. Hence, we assume conservatively that the far-infrared luminosity is derived from star formation in the remaining 70%. Luminosity-density measurements can be translated into a star-formation density using the standard calibration[24] of 1.6–$2.2 \times 10^9\,L_\odot(M_\odot\,\mathrm{yr}^{-1})^{-1}$.

The bright radio-detected submm galaxies presented here represent just 20% of the 850-μm background, yet their estimated star-formation densities at redshifts of 2 and 3 are comparable with those inferred from optical observations[21]. Both of these estimates require corrections: for the optical surveys an increase of a factor of 5 is needed to account for dust obscuration[25], and our submm estimate needs to be corrected by a similar factor to account for spectroscopic incompleteness and sources below our submm flux limit. We find that the submm and Lyman-break populations encompass all of the star formation activity needed to reproduce the star formation history inferred from models of the background radiation and submm counts[4]. Hence, our substantially complete redshift survey provides the strongest evidence for a rapid increase in the density of dusty, very luminous galaxies in the distant Universe. Their density peaks at a redshift $z \approx 2.4$ at a value about 1,000 times greater than
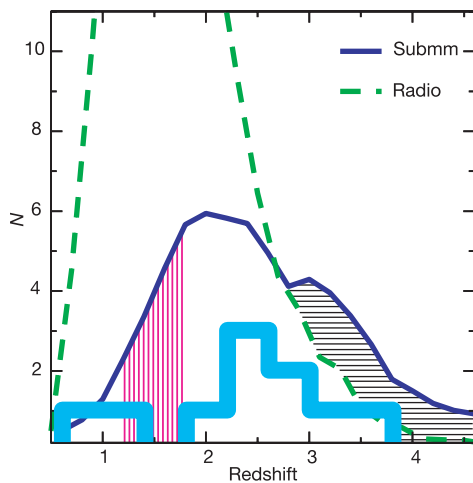
Figure 2 The redshift histogram of our submm galaxy sample (heavy cyan line). We describe the selection effects using an evolving model of the local far-infrared luminosity function[29], in which the dusty galaxies are represented by a range of template spectral energy distributions. The model has been tuned to fit the statistical properties of the submm-radio galaxy population (surface density on the sky and submm–radio colours[29]. Because a range of spectral energy distributions are represented at each galaxy luminosity, a broader redshift distribution results than if the luminosity were tied one-to-one with the dust temperature[23]. We plot the predicted redshift distributions for submm galaxies with flux densities $S_{850\,\mu m} > 5$ mJy (solid blue line) and radio sources with $30\,\mu\mathrm{Jy} < S_{1.4\,\mathrm{GHz}} < 500\,\mu\mathrm{Jy}$ (dashed green line). We expect to miss sources lying between the submm and radio model curves (shaded black) owing to our requirement of a radio detection to pinpoint the submm source. The apparent deficit (shaded magenta) between model and data at $z \approx 1.5$ may be indicative of the difficulty in obtaining spectra in the spectroscopic desert that spans the range $1.2 < z < 1.8$. Note that the models are in good overall agreement with the observed redshift distribution.

letters to nature

the density at the present epoch. Thus we conclude that the balance between the star-formation density in the most luminous dust-obscured versus unobscured galaxies has altered radically over the last 80% of the history of the Universe. □

1. Fixsen, D. J., Dwek, E., Mather, J. C., Bennett, C. L. & Shafer, R. A. The spectrum of the extragalactic far-infrared background from the COBE FIRAS observations. *Astrophys. J.* **508**, 123–128 (1998).
2. Smail, I., Ivison, R. J. & Blain, A. W. A deep submillimeter survey of lensing clusters: a new window on galaxy formation and evolution. *Astrophys. J.* **490**, L5–L8 (1997).
3. Smail, I., Ivison, R. J., Blain, A. W. & Kneib, J.-P. The nature of faint submillimeter-selected galaxies. *Mon. Not. R. Astron. Soc.* **331**, 495–520 (2002).
4. Blain, A. W., Smail, I., Ivison, R. J. & Kneib, J.-P. The history of star-formation in dusty galaxies. *Mon. Not. R. Astron. Soc.* **302**, 632–648 (1999).
5. Barger, A. J., Cowie, L. L. & Richards, E. A. Mapping the evolution of high-redshift dusty galaxies with submillimeter observations of a radio-selected sample. *Astron. J.* **119**, 2092–2109 (2000).
6. Chapman, S. C., Richards, E. A., Lewis, G. F., Wilson, G. & Barger, A. J. The nature of the bright submillimeter galaxy population. *Astrophys. J.* **548**, L147–L151 (2001).
7. Ivison, R. J. *et al.* Deep radio imaging of the SCUBA 8-mJy survey fields: submm source identifications and redshift distribution. *Mon. Not. R. Astron. Soc.* **337**, 1–25 (2002).
8. Boyle, B. J. *et al.* The 2dF QSO redshift survey—I. The optical luminosity function of quasi-stellar objects. *Mon. Not. R. Astron. Soc.* **317**, 1014–1022 (2000).
9. Cowie, L. L., Barger, A. J. & Kneib, J.-P. Faint submillimeter counts from deep 850 micron observations of the lensing clusters A370, A851, and A2390. *Astron. J.* **123**, 2197–2205 (2002).
10. Ivison, R. J. *et al.* A hyperluminous galaxy at z = 2.8 found in a deep submillimetre survey. *Mon. Not. R. Astron. Soc.* **298**, 583–593 (1998).
11. Barger, A. J. *et al.* Redshift distribution of the faint submillimeter galaxy population. *Astron. J.* **117**, 2656–2665 (1999).
12. Ivison, R. J. *et al.* The diversity of SCUBA-selected galaxies. *Mon. Not. R. Astron. Soc.* **315**, 209–221 (2000).
13. Richards, E. A. The nature of radio emission from distinct galaxies: The 1.4 GHz observations. *Astrophys. J.* **533**, 611–630 (2000).
14. Fomalont, E. B., Kellermann, K. I., Partridge, R. B., Windhorst, R. A. & Richards, E. A. The microjansky sky at 8.4 GHz. *Astron. J.* **123**, 2402–2416 (2002).
15. Barger, A. J. *et al.* Submillimetre-wavelength detection of dusty star-forming galaxies at high redshift. *Nature* **394**, 248–251 (1998).
16. Chapman, S. C. *et al.* The properties of microjansky radio sources in the HDF-N, SSA13, and SSA22 fields. *Astrophys. J.* **585**, 57–66 (2003).
17. Scott, S. E. *et al.* The SCUBA 8-mJy survey—I. Submillimetre maps, sources and number counts. *Mon. Not. R. Astron. Soc.* **331**, 817–837 (2002).
18. Chapman, S. C., Lewis, G. F., Scott, D., Borys, C. & Richards, E. A. Understanding the nature of the optically faint radio sources and their connection to the submillimeter population. *Astrophys. J.* **570**, 557–570 (2002).
19. Condon, J. Radio emission from ordinary galaxies. *Annu. Rev. Astron. Astrophys.* **30**, 575–611 (1992).
20. Barger, A. J. *et al.* X-ray, optical and infrared imaging and spectral properties of the 1-Ms Chandra Deep Field North sources. *Astron. J.* **124**, 1839–1885 (2002).
21. Steidel, C. C., Adelberger, K. L., Giavalisco, M., Dickinson, M. & Pettini, M. Lyman-break galaxies at z > 4 and the evolution of the ultraviolet luminosity density at high redshift. *Astrophys. J.* **519**, 1–17 (1999).
22. Steidel, C. *et al.* The population of faint optically-selected AGN at z ∼3. *Astrophys. J.* (in the press); preprint available at http://www.arXiv.org/astro-ph/0205142 (2002).
23. Blain, A. W., Smail, I., Ivison, R. J., Kneib, J.-P. & Frayer, D. T. Submillimeter galaxies. *Phys. Rep.* **369**, 111–196 (2002); preprint available at http://www.arXiv.org/astro-ph/0202228 (2002).
24. Kennicutt, R. C. Star formation in galaxies along the Hubble sequence. *Annu. Rev. Astron. Astrophys.* **36**, 189–232 (1998).
25. Pettini, M. *et al.* The rest-frame optical spectra of Lyman-break galaxies: star formation, extinction, abundances and kinematics. *Astrophys. J.* **554**, 981–1000 (2001).
26. Chapman, S. C., Smail, I., Ivison, R. & Blain, A. The effect of lensing on the identification of SCUBA galaxies. *Mon. Not. R. Astron. Soc.* **335**, 17–21 (2002).
27. Sheinis, A. I. *et al.* ESI, a new Keck Observatory echellette spectrograph and imager. *Publ. Astron. Soc. Pacif.* **114**, 851–865 (2002).
28. Oke, J. B. *et al.* The Keck low-resolution imaging spectrometer. *Publ. Astron. Soc. Pacif.* **107**, 375–385 (1995).
29. Chapman, S. C., Helou, G., Lewis, G. F. & Dale, D. The bi-variate luminosity-colour distribution of IRAS galaxies, and implications for the high redshift Universe. *Astrophys. J.* (in the press); preprint available at http://www.arXiv.org/astro-ph/0301233 (2002).
30. Smail, I. *et al.* A vigorous starburst in the SCUBA galaxy N2_850.4. *Mon. Nat. R. Astron. Soc.* (in the press); preprint available at http://www.arXiv.org/astro-ph/0303128 (2003).

·········

A hidden pseudogap under the 'dome' of superconductivity in electron-doped high-temperature superconductors

L. Alff*, Y. Krockenberger*, B. Welter*, M. Schonecke*, R. Gross*, D. Manske† & M. Naito‡

* Walther-Meissner-Institut, Bayerische Akademie der Wissenschaften, 85748 Garching, Germany
† Freie Universität Berlin, Institut für Theoretische Physik, 14195 Berlin, Germany
‡ NTT Basic Research Laboratories, 3-1 Morinosato, Atsugi, Kanagawa 243, Japan

....

The ground state of superconductors is characterized by the long-range order of condensed Cooper pairs: this is the only order present in conventional superconductors. The high-transition-temperature (high-T_c) superconductors, in contrast, exhibit more complex phase behaviour, which might indicate the presence of other competing ground states. For example, the pseudogap[1,2]—a suppression of the accessible electronic states at the Fermi level in the normal state of high-T_c superconductors—has been interpreted as either a precursor to superconductivity[3,4] or as tracer of a nearby ground state that can be separated from the superconducting state by a quantum critical point[5,6]. Here we report the existence of a second order parameter[7] hidden within the superconducting phase of the underdoped (electron-doped) high-T_c superconductor $Pr_{2-x}Ce_xCuO_{4-y}$ and the newly synthesized electron-doped material $La_{2-x}Ce_xCuO_{4-y}$ (ref. 8). The existence of a pseudogap when superconductivity is suppressed excludes precursor superconductivity as its origin. Our observation is consistent with the presence of a (quantum) phase transition at $T = 0$, which may be a key to understanding high-T_c superconductivity. This supports the picture that the physics of high-T_c superconductors is determined by the interplay between competing and coexisting ground states.

It is well established that above the superconducting transition
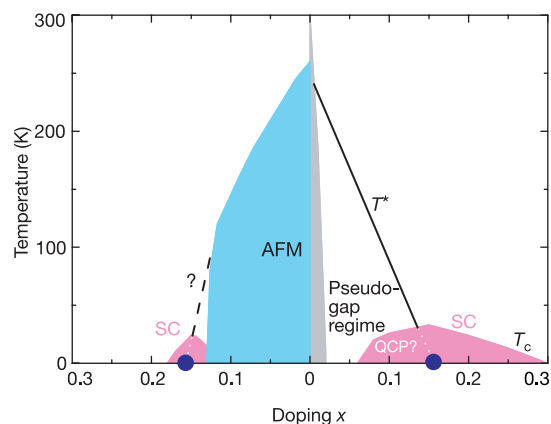
Figure 1 Simplified schematic phase diagram for hole-doped and electron-doped high-T_c superconductors (SC): left, electron-doped $(La,Pr,Nd)_{2-x}Ce_xCuO_{4-y}$; right, hole-doped $La_{2-x}Sr_xCuO_{4-y}$. The exact behaviour of the characteristic pseudogap temperature $T^*(x)$ is under discussion for the hole-doped case and is almost unknown for the electron-doped side. The different decay of antiferromagnetism (AFM) with increased x is due to spin dilution and spin frustration for electron doping and hole doping, respectively. A possible quantum critical point (QCP) is indicated.